Bioactive Materials 9 (2022) 446–460

Contents lists available at ScienceDirect

Bioactive Materials

journal homepage: www.sciencedirect.com/journal/bioactive-materials

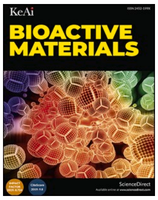

Biofunctionalized composite scaffold to potentiate osteoconduction, angiogenesis, and favorable metabolic microenvironment for osteonecrosis therapy

Tongtong Zhu [a], Mengyang Jiang [c], Mingran Zhang [a,b], Liguo Cui [b], Xiaoyu Yang [b], Xukai Wang [a], Guangyao Liu [a,**], Jianxun Ding [b,*], Xuesi Chen [b]

[a] *Department of Orthopedics, China-Japan Union Hospital of Jilin University, 126 Xiantai Street, Changchun, 130033, PR China*
[b] *Key Laboratory of Polymer Ecomaterials, Changchun Institute of Applied Chemistry, Chinese Academy of Sciences, 5625 Renmin Street, Changchun, 130022, PR China*
[c] *Department of Ophthalmology, The Second Hospital of Jilin University, 218 Ziqiang Road, Changchun, 130041, PR China*

ARTICLE INFO

Keywords:
Biofunctionalized scaffold
Osteoconduction
Angiogenesis
Favorable metabolic microenvironment
Osteonecrosis therapy

ABSTRACT

Osteonecrosis is a common orthopedic disease in clinic, resulting in joint collapse if no appropriate treatment is performed in time. Core decompression is a general treatment modality for early osteonecrosis. However, effective bone regeneration in the necrotic area is still a significant challenge. This study developed a biofunctionalized composite scaffold (PLGA/nHA$_{30}^{\mathrm{VEGF}}$) for osteonecrosis therapy through potentiation of osteoconduction, angiogenesis, and a favorable metabolic microenvironment. The composite scaffold had a porosity of 87.7% and compressive strength of 8.9 MPa. PLGA/nHA$_{30}^{\mathrm{VEGF}}$ had an average pore size of 227.6 μm and a water contact angle of 56.5° with a sustained release profile of vascular endothelial growth factor (VEGF). After the implantation of PLGA/nHA$_{30}^{\mathrm{VEGF}}$, various osteogenic and angiogenic biomarkers were upregulated by 2–9 fold compared with no treatment. Additionally, the metabolomic and lipidomic profiling studies demonstrated that PLGA/nHA$_{30}^{\mathrm{VEGF}}$ effectively regulated the multiple metabolites and more than 20 inordinate metabolic pathways in osteonecrosis. The excellent performances reveal that the biofunctionalized composite scaffold provides an advanced adjuvant therapy modality for osteonecrosis.

1. Introduction

Osteonecrosis caused by trauma, glucocorticoid abuse, or alcoholism is a common clinical orthopedic disease, resulting in progressive bone destruction and eventually joint collapse [1,2]. Cases of osteonecrosis in the United States exceeded 20,000 per year, while there were approximately 150,000 cases in China [3,4]. Steroid-induced osteonecrosis is one of the most common forms. 47.4% of patients with non-traumatic osteonecrosis have received steroid treatment, while 5%–40% of patients receiving steroid therapy developed a certain degree of osteonecrosis [5,6].

Core decompression combined with bone grafting is an effective strategy for early osteonecrosis therapy in clinical practice. However, the obstacle of bone regeneration after core decompression is still a severe challenge [7,8], which is affected by the adverse microenvironments in osteonecrosis [2]. Autogenous bone grafting is an effective strategy for promoting bone regeneration, while the restricted source of the donor, prolonged operation time, risk of infection, and possible morbidity at the donor site restrict its clinical application [9].

The composite scaffolds are expected to be a promising device for regulating the microenvironments in osteonecrosis and overcoming challenges associated with bone regeneration. Many organic (*e.g.,* poly (lactide-*co*-glycolide) (PLGA), poly(ε-caprolactone), polylactide, and chitosan), inorganic (*e.g.,* nano-hydroxyapatite (nHA), β-tricalcium calcium phosphate, ceramic, and Ti), and composite materials have elicited increasing attention as matrices for bone tissue engineering scaffolds. This is because of their outstanding biocompatibility, controllable degradability, easy processability, excellent mechanical properties, osteoconductivity, and the ability to promote bone regeneration [2,9–12]. However, the main limitation of organic and inorganic

---

Peer review under responsibility of KeAi Communications Co., Ltd.
* Corresponding author.
** Corresponding author.
E-mail addresses: gyliu@jlu.edu.cn (G. Liu), jxding@ciac.ac.cn (J. Ding).

https://doi.org/10.1016/j.bioactmat.2021.08.005
Received 31 March 2021; Received in revised form 1 August 2021; Accepted 3 August 2021

composite scaffolds in osteonecrosis treatment is insufficient biofunctionalization, such as angiogenic modification.

During bone regeneration in osteonecrosis, vascular remodeling is a critical factor, and osteogenesis and angiogenesis support each other in the process of bone remodeling [13]. The formation of blood vessels provides nutrients for bone remodeling. Some osteogenic proteins also have the effect of promoting angiogenesis, such as osteocalcin (OCN), and the vascular network in the scaffold helps its integration with the host bone [14,15]. Angiogenic factors, such as vascular endothelial growth factor (VEGF), erythropoietin, and platelet-rich plasma, promote the proliferation and migration of endothelial cells, enhance capillary formation, contribute to the vascularization inside the scaffold and new bone, accelerate osteogenic differentiation, and calibrate the balance between osteogenic and lipogenic differentiation [2,8]. Therefore, angiogenic factor-incorporated composite scaffolds will serve as a promising biofunctionalized device for osteonecrosis therapy.

Osteonecrosis always has complex microenvironmental changes, including apoptosis of osteocytes and osteoblasts, impaired function of vascular endothelial cells, imbalance of osteogenic and adipogenic differentiation of bone marrow-derived mesenchymal stem cells (BMSCs), abnormal lipid metabolism, and so forth [16]. The recently published studies mainly used metabolomics to detect the differential metabolites in the blood and urine of patients and animal models with osteonecrosis, but this is not accurate enough to reflect the metabolic disorders in the bone tissue microenvironments. Meanwhile, few studies have explored the influence of the local metabolic microenvironment regulation on osteonecrosis therapy.

In this study, we prepared a VEGF-functionalized PLGA/nHA composite porous scaffold (PLGA/nHA$_{30}$^{VEGF}) for synergistic therapy of osteonecrosis through the osteoconductivity of synthetic nHA, the angiogenic ability of VEGF, and the metabolic regulation of biofunctionalized scaffold (Scheme 1). The chemical and physical properties of the scaffolds were characterized, and then the scaffolds were implanted into the rabbit osteonecrosis model for evaluation of their osteogenic and angiogenic capability. Additionally, the effect of the optimized biofunctionalized scaffold on the reversal of adverse microenvironments in osteonecrosis was revealed by metabolomic and lipidomic profiling. The biofunctionalized composite scaffold will serve as an effective candidate for osteonecrosis therapy through the potentiation of osteoconduction, angiogenesis, and a favorable metabolic microenvironment.

2. Materials and methods

2.1. Fabrication of composite scaffolds with different nano-hydroxyapatite contents

The composite scaffolds with 10 wt% nHA (PLGA/nHA$_{10}$) and 30 wt% nHA (PLGA/nHA$_{30}$) were provided by Changchun SinoBiomaterials Co., Ltd. (Changchun, P. R. China). Briefly, two kinds of scaffolds were both prepared by the phase separation/particle leaching method. First, PLGA was added in *N*,*N*-dimethylformamide (DMF) and stirred for 3–4 h until PLGA was entirely dissolved. In addition, nHA was added into DMF and sonicated for 15 min to make it evenly dispersed. The two solutions described above were mixed to prepare a PLGA solution (20 wt%), and nHA accounted for 10 wt% or 30 wt% of PLGA. Then, the sodium

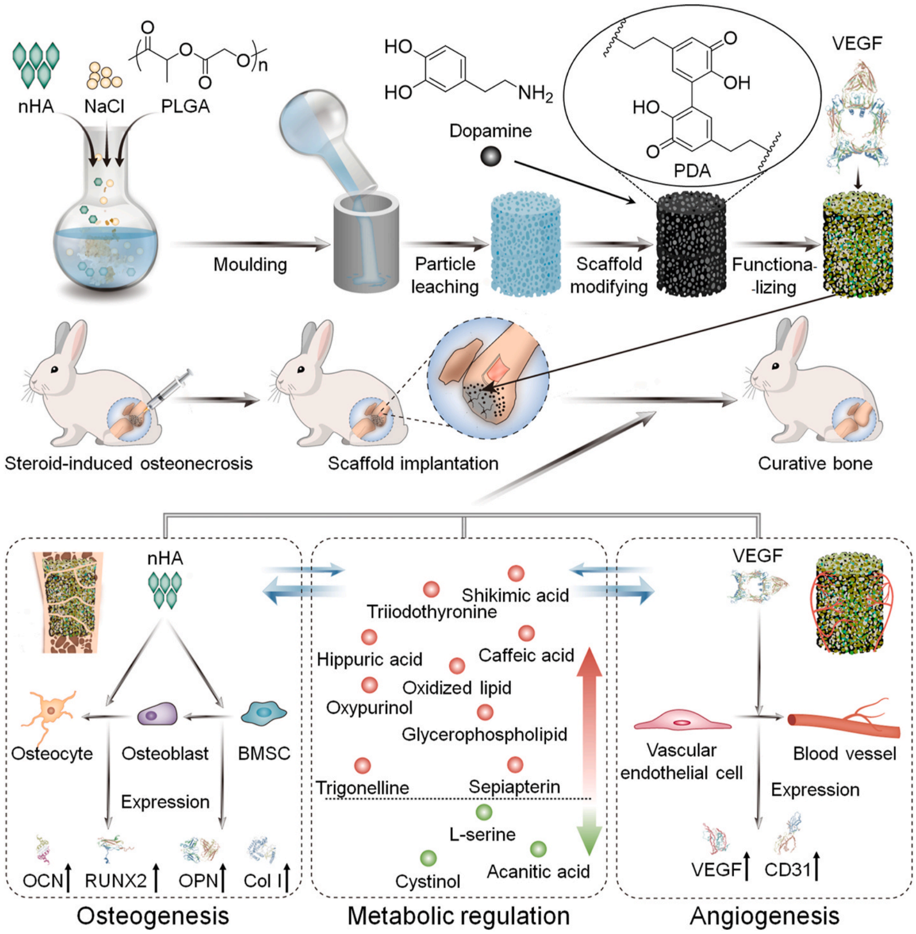

Scheme 1. A biofunctionalized composite scaffold to potentiate osteoconduction, angiogenesis, and a favorable metabolic microenvironment for osteonecrosis therapy.

chloride (NaCl) particle (200–400 μm) was added to the PLGA/nHA solution and stirred thoroughly. The ratio of the total mass of NaCl particle to that of nHA+PLGA was 9:1. The evenly mixed solvent was poured into the mold and allowed to stand for 2 h in the aseptic operation table to pre-solidify the composite. After that, the composite was immersed in sterilized deionized water and slowly stirred for two days at 37 °C. The sterilized deionized water was replaced every 6 h, and contamination was carefully prevented during the replacement process. After the composite was freeze-dried, it was sterilized with ethylene oxide.

2.2. Fabrication of biofunctionalized composite scaffold

The sterilized cylindrical PLGA/nHA_{30} (diameter = 4.6 mm and length = 8.0 mm) was immersed in the dopamine (DA) solution (4.0 mg mL^{-1} in 10.0 mM Tris buffer, pH 8.5). The solution with scaffold was placed under vacuum until the bubbles around the scaffold disappeared and then gently shaken for 4 h at room temperature after adding air. The scaffold was then washed with Milli-Q water thrice to remove the free DA and obtain the polydopamine (PDA)-functionalized PLGA/$nHA_{30}{}^{PDA}$. PLGA/$nHA_{30}{}^{PDA}$ was dried under nitrogen (N_2) and then immersed in VEGF solution (5.0 μg mL^{-1}). Next, the solution with scaffold was shaken for 12 h at 4 °C to obtain the biofunctionalized composite scaffold PLGA/$nHA_{30}{}^{VEGF}$. Using the same protocol, the bovine serum albumin (BSA; 50.0 μg mL^{-1}) was used to prepare PLGA/$nHA_{30}{}^{BSA}$ as a control.

2.3. Physicochemical properties of composite scaffolds

The detailed characterizations of pore structures, hydrophilicity, mechanical properties, biodegradability, and protein loading and release of biofunctionalized composite scaffolds are described in Supplementary data.

2.4. Animal study

All animal experiments were performed in compliance with the principles of the Institutional Animal Care and Use Committee of Jilin University. A total of 77 adult male Japanese white rabbits (aged 22–26 weeks old and weighing 2.8–4.0 kg) were fed with a standard laboratory diet at the Animal Center of Jilin University. Of these, 21 rabbits were used to prove the successful establishment of osteonecrosis model, 32 rabbits were used to observe bone regeneration and vascular regeneration experiments, and 24 rabbits were used for metabolomics profiling.

2.4.1. Construction of rabbit osteonecrosis model

The rabbit osteonecrosis model was constructed according to previously reported protocols with appropriate modifications [17,18]. In detail, the model was established by intramuscular injection of 40.0 mg per kg body weight (mg (kg BW)$^{-1}$) methylprednisolone (MP) into the right gluteus medius every day for three times. At each predetermined time point, the hematological test, radiologic analysis, and histopathological examination were performed to monitor the pathogenesis of osteonecrosis.

2.4.2. Treatment of osteonecrosis with biofunctionalized composite scaffold

Two weeks after the induction of osteonecrosis, 32 rabbits were divided into four groups ($n = 8$): Control, PLGA/nHA_{10}, PLGA/nHA_{30}, and PLGA/$nHA_{30}{}^{VEGF}$. After anesthetization with 10.0 mg (kg BW)$^{-1}$ of xylazine hydrochloride intramuscularly, the lateral side of the rabbit's left knee was exposed, sterilized, and covered with sterile sheets routinely. A 3 cm longitudinal skin incision along the distal femur was created, and the subcutaneous tissue and fascia were separated to expose the femoral condyle. An electric drill was used to create a defect channel (5.2 mm in diameter and 8–10 mm in length) at the center of the lateral femoral condyle. Different scaffolds were implanted according to the following groupings: the drilled area without implantation (Control), the drilled area implanted with PLGA/nHA_{10} (PLGA/nHA_{10}), the drilled area implanted with PLGA/nHA_{30} (PLGA/nHA_{30}), and the drilled area implanted with PLGA/$nHA_{30}{}^{VEGF}$ (PLGA/$nHA_{30}{}^{VEGF}$). After the incision was washed with normal saline, it was sutured layer by layer with absorbable sutures. Intramuscular injection of 400,000 units of penicillin was performed 2 h before surgery and every day for three days after surgery to prevent infection.

2.4.3. Hematological examinations

Alkaline phosphatase (ALP) and osteocalcin (OCN), two serum markers of bone formation, were detected using a biochemistry analyzer (Chemray 800, Rayto, Shanghai, P. R. China) and an enzyme-linked immunosorbent assay (ELISA) kit in eight weeks after the operation, respectively ($n = 5$). The whole blood samples were clotted in a water bath for about 30 min at 37 °C and then overnight at 4 °C. After centrifugation for 5 min at 1500 r min^{-1}, blood serum was isolated and preserved at −80 °C. All procedures were strictly performed according to the protocols provided by the manufacturers. For ELISA detection, we measured the absorbance value at 450 nm of the samples using a microplate reader (SPARK, TECAN, Switzerland). All samples were detected in triplicate.

2.4.4. Micro-CT analysis on new bone formation within bone tunnels

Eight rabbits in each group were sacrificed 12 weeks after the operation. Six rabbits remained in each group after excluding rabbits with joint contractures, infections, or lower-limb paralysis. The rabbits were processed for micro-CT and then for histology analysis after being fixed with 4% (*W/V*) PBS-buffered paraformaldehyde. The regenerated level of new bone tissue was assessed *via* radiographic analysis using micro-CT (Skyscan1172, Bruker, Karlsruhe, Germany). Scanning and calculation parameters are mentioned in Supplementary data. We set the region of interest (ROI) as the bone drilling area (diameter = 5.2 mm). Bone volume (BV, mm^3), percent bone volume (BV/TV, %), trabecular number (Tb.N, mm^{-1}), trabecular thickness (Tb.Th, mm), bone surface (BS, mm^2), and bone surface/volume ratio (BS/TV, mm^{-1}) within the ROI were measured.

2.4.5. Histopathological and histometric analysis

Ethylenediaminetetraacetic acid (EDTA) solution (10% *W/V*) was used to decalcify the obtained bones, which were then embedded in paraffin blocks and cut into 5-μm thick sections for hematoxylin and eosin (H&E) staining, Masson trichrome staining, Goldner trichrome staining, and immunohistochemistry staining. The expression of OCN, runt-related transcription factor 2 (Runx2), osteopontin (OPN), type I collagen (Col I), VEGF, and CD31 within implantation regions was detected by immunohistochemistry staining, which was relatively quantified by using ImageJ software to calculate the staining intensity/stained area (1.52 V, Wayne Rasband, Softonic International, Spain).

2.5. Metabolomic and lipidomic profiling of bone specimens

Twenty-four rabbits were divided into three groups ($n = 8$): normal, model, and treatment groups. The normal group received a saline injection. The model group was given an MP injection. The treatment group was treated with surgery and implanted with PLGA/$nHA_{30}{}^{VEGF}$ two weeks after the induction of osteonecrosis. Eight weeks after the operation, the rabbits were sacrificed ($n = 8$), and the femoral condyles were harvested. We removed the soft tissue and periosteum, split the femoral condyles along the sagittal plane using a bone saw, and washed away the bone marrow with normal saline. Next, we took out the internal cancellous bone and the biofunctionalized composite scaffolds with a rongeur and stored them in liquid N_2. Finally, the collected samples were used for metabolomic and lipidomic profiling (Metware Biotechnology Co. Ltd., Wuhan, P. R. China).

2.6. Statistical analysis

Data were presented as mean ± standard deviation (SD). The analysis was performed using one-way ANOVA and Student's *t*-tests (Version 6.01 software, GraphPad Software, Inc., USA). $^{*}P < 0.05$ was considered to be statistically significant, and $^{**}P < 0.01$, $^{***}P < 0.001$, and $^{****}P < 0.0001$ were considered to be highly significant.

3. Results and discussion

3.1. Fabrication and characterizations of composite scaffolds

The bone-substitute materials should have a porous three-dimensional (3D) structure with sufficient porosity and pore size to provide enough space for the stem cells, osteocytes, osteoblasts, and vascular endothelial cells. According to the routine scan (Fig. S1, Supplementary data) and 3D reconstructed micro-CT images (Fig. 1A), each type of scaffold was shown to have evenly distributed porous structures on the surface and inside, and there were interconnected structures between the pores. The porous interpenetrating structures of scaffolds were confirmed using scanning electronic microscopy (SEM) images (Fig. 1B). These structures not only enhanced new bone growth and blood vessel formation but were also conducive for protein loading and release [2,19]. As shown in Fig. 1C, a large amount of uniform fluorescently-labeled protein adhered to the inside of the scaffold. It demonstrated that due to the open structure of the scaffold, the protein could penetrate to the scaffold's inner surface instead of only forming a coating on the scaffold's outer surface.

PLGA/nHA$_{10}$ and PLGA/nHA$_{30}$ had similar porosities, 87.7% ± 0.06% and 87.4% ± 0.54% ($n = 3$). The results indicated that the change of proportion of nHA did not affect the porosities of composite scaffolds. Using SEM, we observed that the pore sizes of PLGA/nHA$_{10}$, PLGA/nHA$_{30}$, and PLGA/nHA$_{30}^{BSA}$ were 239.4 ± 18.16 μm, 225.9 ± 28.76 μm, and 229.3 ± 12.11 μm, respectively (Fig. 1D). There was no significant difference among them, which demonstrated that neither the increase in nHA content nor the addition of PDA and protein had obvious effects on

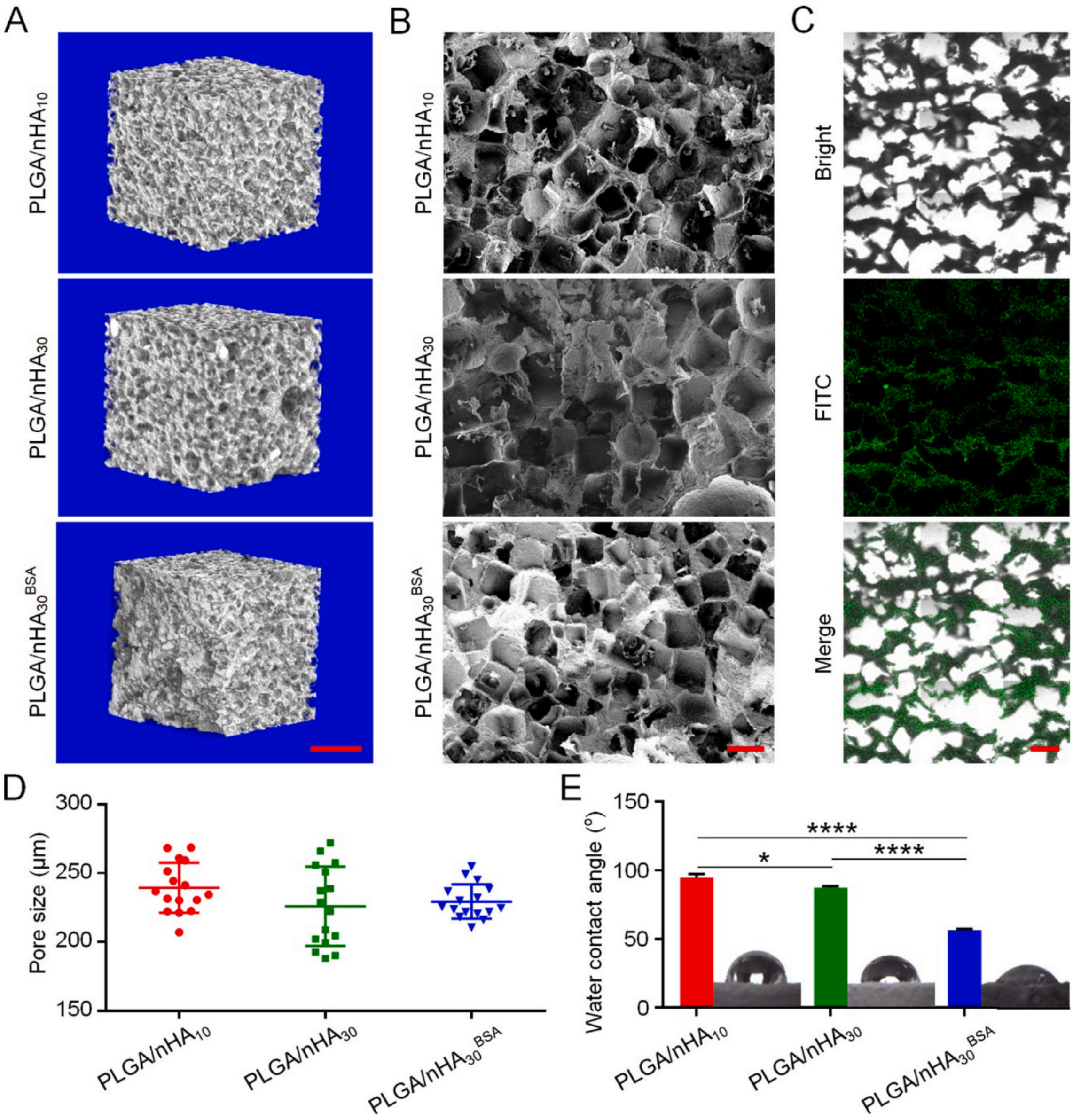

Fig. 1. Microstructures of composite scaffolds. (A) 3D reconstruction of micro-CT images of three composite scaffolds. Scale bar = 1 mm. (B) SEM imaging of three composite scaffolds. Scale bar = 200 μm (C) CLSM imaging of PLGA/nHA$_{30}^{BSA}$. Scale bar = 300 μm (D) Pore sizes of three scaffolds. (E) Water contact angles of three scaffolds. Data are represented as mean ± SD ($n = 3$; $^{*}P < 0.05$, $^{****}P < 0.0001$).

the scaffold's pore size. Zhang *et al.* summarized the effect of different pore sizes in bone tissue engineering and found that if the pore size was between 100.0 and 300.0 μm, it was conducive to cell penetration, migration, growth, and the best angiogenesis [20]. On this basis, the composite scaffolds we designed had excellent porosity, pore size, and an interconnected porous structure, which helped achieve rapid angiogenesis and promoted high levels of oxygen delivery to the necrotic area to overcome the harmful microenvironments and stimulated bone regeneration in osteonecrosis.

The composite scaffold with outstanding hydrophilicity is conducive to the adhesion of cells [12]. The water contact angles of PLGA/nHA$_{10}$ and PLGA/nHA$_{30}$ were 94.7° and 87.3°, respectively (Fig. 1E). The increase of nHA content improved the hydrophilicity of composite scaffold because of the presence of hydrophilic P–OH group on the surface of nHA [21]. Moreover, with the addition of PDA and protein, the scaffold hydrophilicity was greatly improved, and the water contact angle of PLGA/nHA$_{30}$^{BSA} was 56.5°. This was because PDA was rich in hydrophilic functional groups, such as amino-functional and carboxyl-functional groups [22].

During osteonecrosis treatment, the newly formed woven bone tissue is about to be remodeled into trabecular bone, and the new blood vessels are sensitive to external pressure and are easily damaged, ultimately resulting in repair failure [23]. Therefore, the ideal scaffold for osteonecrosis therapy should provide initial support with similar mechanical performance to the cancellous bone [7,17]. From the mechanical test, the compressive strength and modulus of PLGA/nHA$_{10}$ were 4.9 ± 0.42 and 9.6 ± 2.78 MPa, and those of PLGA/nHA$_{30}$ were 8.9 ± 2.15 and 35.1 ± 11.00 MPa, respectively (Figs. S2A and B, Supplementary data). These values indicated that the developed scaffolds had an excellent mechanical performance. Moreover, the compressive strength and modulus of PLGA/nHA$_{30}$ were higher than those of PLGA/nHA$_{10}$, presumably because of the increase in nHA content.

The proper biodegradability of scaffolds used for bone tissue engineering is one of the prerequisites. This allows for new bones to replace scaffolds and ultimately repair bone defects. The *in vitro* degradation processes of PLGA/nHA$_{10}$, PLGA/nHA$_{30}$, and PLGA/nHA$_{30}$^{BSA} were observed by micro-CT and weight loss. In the first 18 days, the three scaffolds had no apparent weight loss. After that, the weight of the three scaffolds began to decline at an accelerated rate, and the weight reduction of PLGA/nHA$_{30}$^{BSA} was significantly higher than those of the other two scaffolds (Fig. 2A). This might have resulted from the scaffold modification by PDA. The inherent hydrophobicity of PDA allows it to perform the task of degrading stimuli. Additionally, active oxygen, such as oxygen species and free radicals, triggers the oxidative biodegradation of PDA [22]. Throughout the degradation process, the pH value of each degradation product solution was maintained between 6 and 7, and

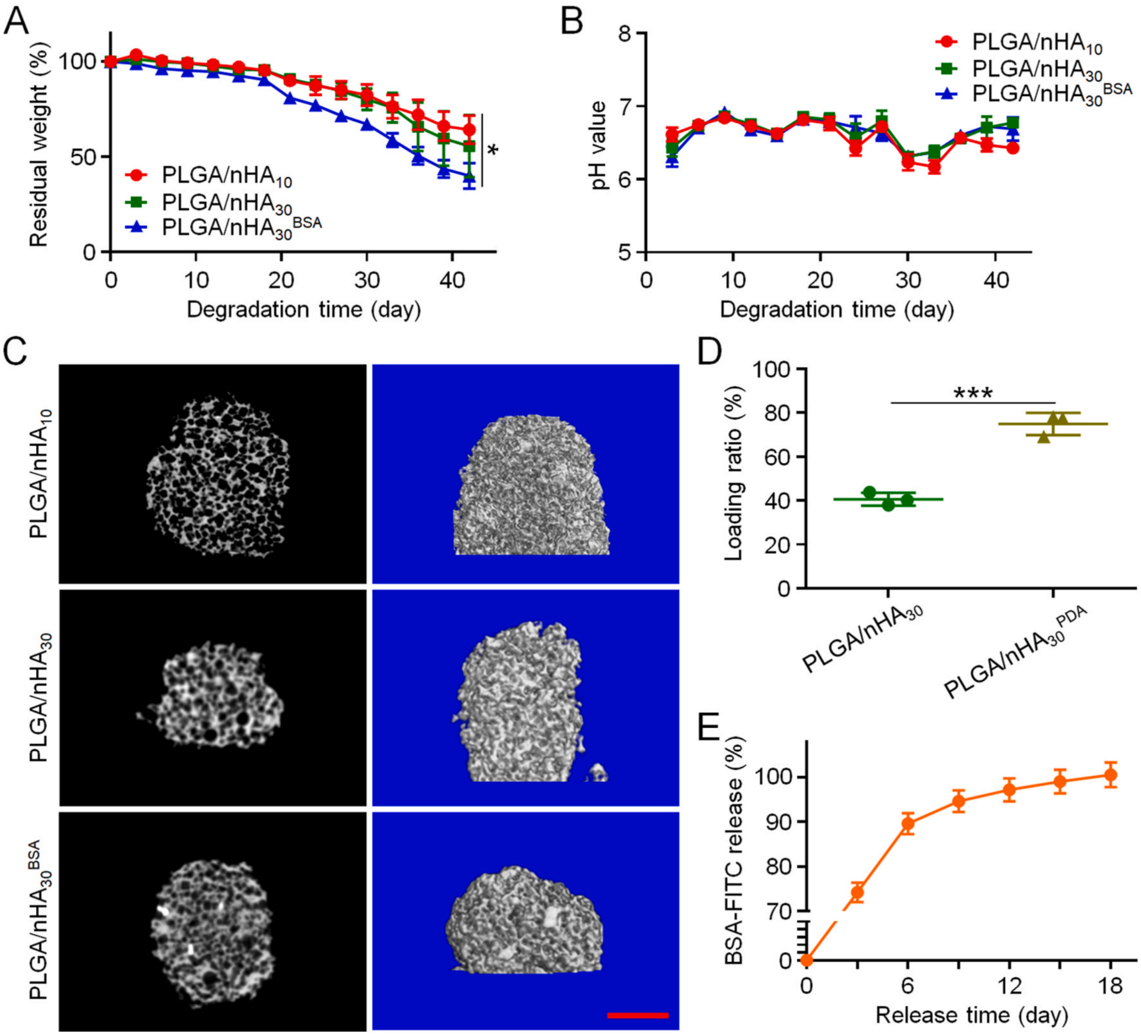

Fig. 2. *In vitro* degradation, and protein loading and release of scaffolds. (A) Weight changes of three composite scaffolds during degradation. (B) Alteration of pH value in medium during scaffold degradation. (C) Routine scan and 3D reconstruction micro-CT images of PLGA/nHA$_{10}$, PLGA/nHA$_{30}$, and PLGA/nHA$_{30}$^{BSA} after 42 days of degradation. Scale bar = 2 mm (D) Protein loading rates of PLGA/nHA$_{30}$ and PLGA/nHA$_{30}$^{PDA} (E) Accumulated release of BSA-FITC from PLGA/nHA$_{30}$^{BSA}. Data are represented as mean ± SD ($n = 3$; $^{*}P < 0.05$, $^{***}P < 0.001$).

there was no significant difference between them (Fig. 2B). This implied that the by-products of scaffold degradation were at a proper pH, thereby partly controlling the generation of unfavorable microenvironments for cell survival. Moreover, through the micro-CT analysis, we found that these three scaffolds still maintained the integrity of the internal pore structure after degradation (Fig. 2C). This is one of the main requirements for the application of scaffolds in osteonecrosis [2].

Inspired by the bio-adhesion principles observed in marine mussels, PDA has been extensively used to modify the surface of materials and immobilize proteins. The scaffolds modified by PDA effectively increased the protein load rate from 40.6% to 78.1% (Fig. 2D). The *in vitro* cumulative release time curve of BSA-FITC conjugated to PLGA/nHA_{30}^{BSA} demonstrated continuous protein release for 18 days (Fig. 2E). Biofunctionalized composite scaffolds realized efficient loading and sustained protein release, contributing to rapid blood vessel formation, thereby accelerating bone regeneration.

3.2. Evaluation of biofunctionalized composite scaffolds for osteonecrosis therapy

The osteonecrosis model of rabbit was constructed by intramuscular injection of 40.0 mg (kg BW)$^{-1}$ MP into the right gluteus medius every day three times. At 2, 6, 8, 10, and 12 weeks post-injection, the successful construction of the rabbit osteonecrosis model was confirmed by pathological assessment, imaging, and hematological analysis.

Two weeks after the induction of osteonecrosis, we simulated core decompression at the femoral condyle and implanted the biofunctionalized composite scaffold. We strictly implemented sterile procedures during the operation and implanted the scaffold to the correct position, where no apparent active bleeding was observed (Fig. S3, Supplementary data). We detected ALP and OCN levels in the serum in eight weeks post-implantation of the biofunctionalized scaffolds (Fig. S4, Supplementary data). The serum ALP and OCN levels in the PLGA/nHA_{30}^{VEGF} group were significantly higher than those in the undecorated composite scaffolds and control groups ($P < 0.05$). However, the levels of the two serum markers of the PLGA/nHA_{10} and PLGA/nHA_{30} groups were almost same as those of the control group ($P > 0.05$). Therefore, we inferred that the undecorated composite scaffold did not play a prominent role in promoting early bone regeneration in osteonecrosis. In contrast, the biofunctionalized composite scaffold had a significant role in the process.

Twelve weeks after the scaffolds were implanted, we sacrificed the rabbits, collected the femoral condyles, and used imaging and pathological detection methods to evaluate bone regeneration. We conducted a comprehensive micro-CT analysis through routine scanning and three-dimensional (3D) reconstruction (Fig. 3A). Only a minimal amount of mineralized tissue was observed in the control group, and most of this was confined to the edge of the defect area. The new bone trabecula was discontinuous, slender, and sparse. Both defect areas were reduced in the PLGA/nHA_{10} and PLGA/nHA_{30} groups, and continuous mineralized bone tissues were observed around the scaffolds. Compared with that of the control group, the bone trabecula was thicker and denser, and there was also a small amount of scattered mineralized tissue inside the scaffold. The PLGA/nHA_{30}^{VEGF} group had the most significant amount of mineralized bone tissue around and inside the scaffold. The trabecular bone was closely connected, and some areas were connected to larger pieces and spread inside the scaffold.

We utilized five bone morphological parameters, BV, BV/TV, Tb.N, Tb.Th, and BS/TV for quantitative analysis of bone regeneration (Fig. 3B–F). The BV and BV/TV of PLGA/nHA_{10} (BV, 27.58 mm^3; BV/TV, 26.46%), PLGA/nHA_{30} (BV, 31.34 mm^3; BV/TV, 29.24%), and PLGA/nHA_{30}^{VEGF} groups (BV, 43.48 mm^3; BV/TV, 41.72%) were significantly higher than those of the control group (BV, 3.43 mm^3; BV/TV, 3.29%). The value of PLGA/nHA_{30}^{VEGF} group was 12 times higher than that of the control group ($P < 0.0001$) and 1.4 times higher than those of the undecorated composite scaffolds. The Tb.N of control group was 0.20 mm^{-1}, which was significantly lower than 1.47 mm^{-1} of PLGA/nHA_{10} group ($P < 0.001$) and 1.66 mm^{-1} of PLGA/nHA_{30} group ($P < 0.01$), and was only one-eighth the value of PLGA/nHA_{30}^{VEGF} group (1.84 mm^{-1}, $P < 0.0001$). Tb.Th was higher in the PLGA/nHA_{30}^{VEGF} group compared with those in the control (higher by 38%), PLGA/nHA_{10} (higher by 27%), and PLGA/nHA_{30} groups (higher by 28%) ($P < 0.05$). BS/TV of the PLGA/nHA_{10}, PLGA/nHA_{30}, and PLGA/nHA_{30}^{VEGF} groups were 5.26, 6.38, and 6.99 mm^{-1}, and these were 6, 7, and 8 times larger when compared with the control group (0.83 mm^{-1}), respectively. Compared with the control group, the synergistic treatment of PLGA/nHA_{30}^{VEGF} more effectively promoted bone regeneration. Additionally, it enhanced the continuity between the new bone trabeculae, increased the thickness and density of bone trabeculae, and was more in line with the mechanical properties required for osteonecrosis therapies.

The histopathological analysis further confirmed the results. H&E staining revealed that the edges and center of drilled area in the control group were filled with bone marrow tissue containing many fat cells. Only a small amount of scattered new bone tissues could be observed, and few blood vessels were found inside or around the new bone tissue (Fig. 4A). In the PLGA/nHA_{10} and PLGA/nHA_{30} groups, we observed a regular trabecular bone structure and new blood vessels forming around the composite scaffolds. Some cartilage structures, representing immature bone tissue, and a small number of bone tissues and new blood vessels were also formed inside the composite scaffolds. In the PLGA/nHA_{30}^{VEGF} group, the largest area of newly formed bone trabeculae and the highest number of vascular structures were observed both around and inside the biofunctionalized composite scaffold. Additionally, the bone trabeculae were arranged regularly and were the thickest in this group. In some regions, large areas of new bone tissue completely replaced the scaffold. In all the scaffold groups, we observed that the new bone grew from the scaffold periphery to the interior, which fully demonstrated the osteoconductivity of scaffolds. Of course, the PLGA/nHA_{30}^{VEGF} group also had the best bone ingrowth.

We conducted a quantitative analysis of the number of the newly formed blood vessels and found that the value in the PLGA/nHA_{30}^{VEGF} group was approximately three times the value in the undecorated composite scaffold groups (Fig. 4B). The composite porous scaffold promoted bone regeneration to a greater extent. The VEGF-functionalized composite scaffolds further improved this effect and significantly accelerated vascular regeneration. We inferred that the osteoconduction and angiogenesis ability of the biofunctionalized composite scaffold had a synergistic effect. Therefore, the repair effect was more remarkable than those of the undecorated composite scaffolds.

We observed and quantitatively analyzed the areas of mature and immature bone tissues in the new bone in each group by Masson trichrome staining. Fig. 4C and D shows that the largest area of newly formed bone tissue, which included mature (red staining) and immature bone (blue staining) tissue, was observed in the PLGA/nHA_{30}^{VEGF} group ($P < 0.001$). Specifically, the PLGA/nHA30VEGF group's value was about two times higher than that of the undecorated composite scaffold groups and almost four times higher than that of the control group in terms of the total new bone area or mature new bone area. Goldner staining showed matching results, and the PLGA/nHA_{30}^{VEGF} group had the most mineralized bone tissue (green staining) and osteoid (red staining), as depicted in Fig. S5, Supplementary data. Interestingly, there was no significant difference in the total new bone tissue between the PLGA/nHA_{30} and PLGA/nHA_{10} groups, while the former groups showed a higher amount of mature bone tissue ($P < 0.01$). The increased content of nHA resulted in the earlier appearance of new bone. On this basis, the addition of VEGF promoted neovascularization in the early stage, promoting bone tissue formation and increasing mature bone tissue.

To explore the vascularization ability of PLGA/nHA_{30}^{VEGF}, we used immunohistochemistry to evaluate angiogenesis further. Perhaps because steroids reduce nitric oxide (NO) activity and induce oxidative stress, osteonecrosis will lead to apoptosis of vascular endothelial cells

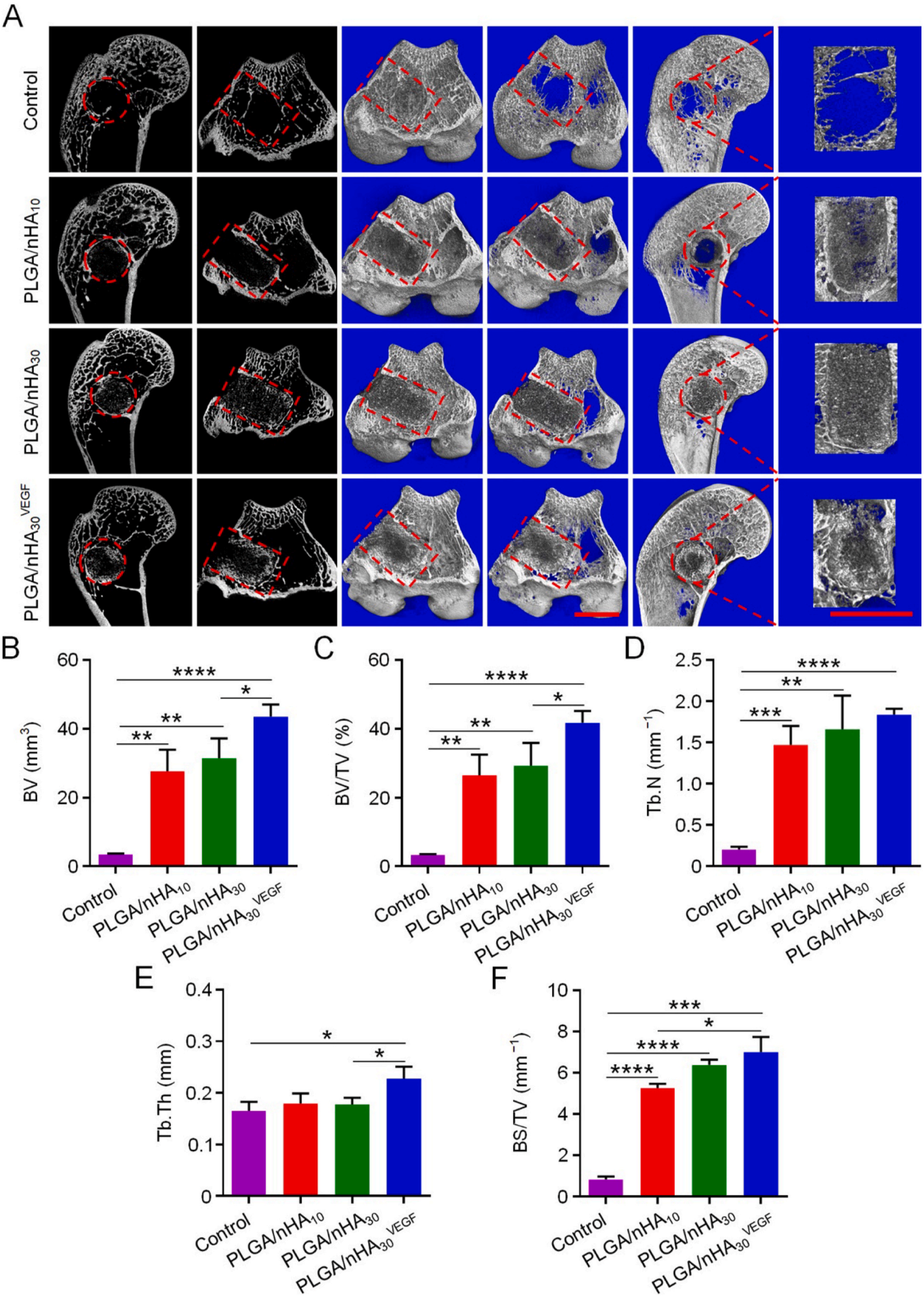

Fig. 3. Micro-CT detection of new bone formation in drill tunnel. (A) Routine scanning and 3D reconstruction micro-CT images of femoral condyles after treatments. The red circle and square indicate ROI. Scale bar = 5 mm. (B–F) Quantitative analysis of bone microstructural parameters in ROI. Data are represented as mean ± SD ($n = 3$; $^*P < 0.05$, $^{**}P < 0.01$, $^{***}P < 0.001$, $^{****}P < 0.0001$). (For interpretation of the references to colour in this figure legend, the reader is referred to the Web version of this article.)

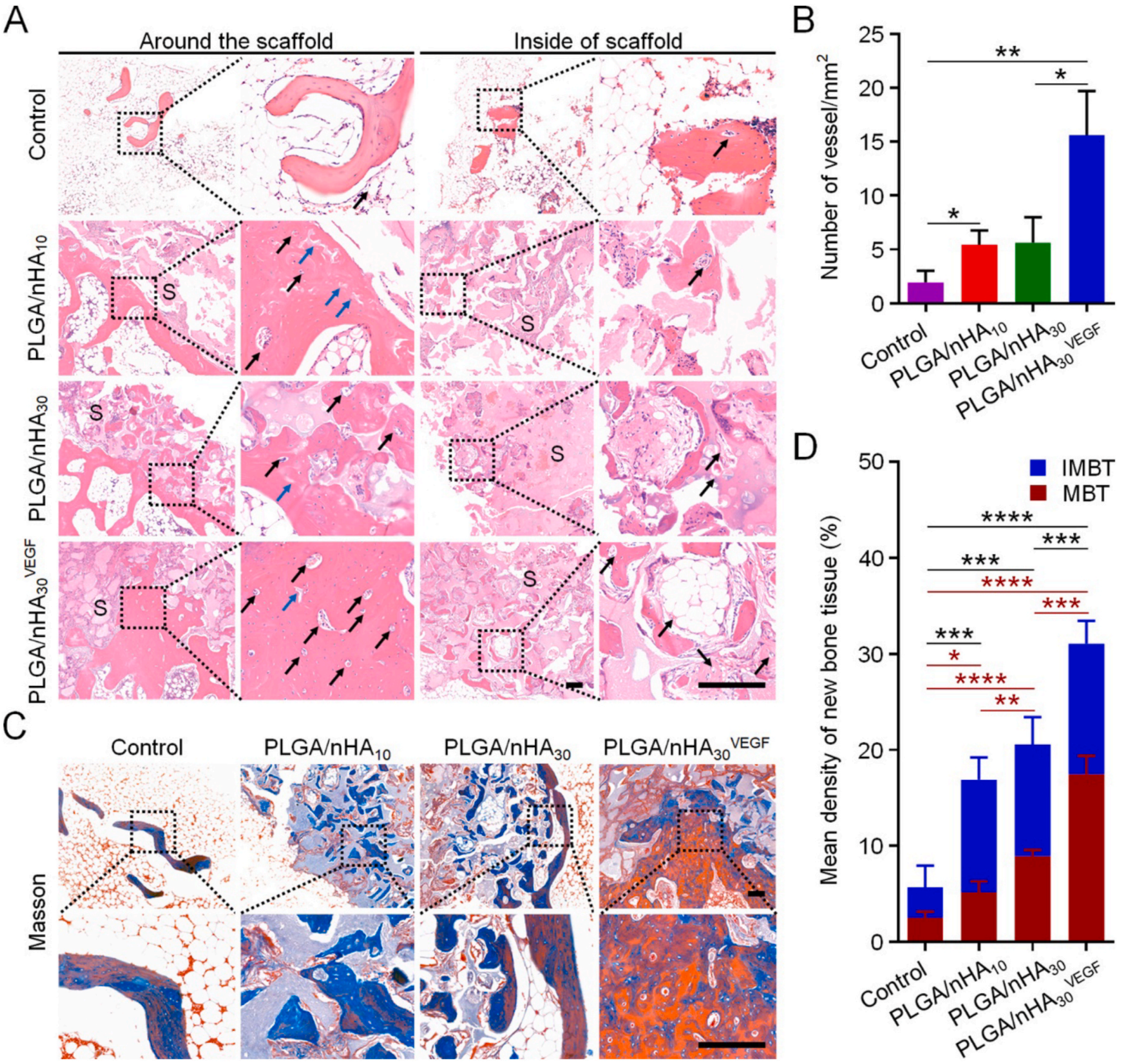

Fig. 4. Histopathological analysis of new bone formation after scaffold implantation. (A) H&E staining showed the formation of new bone and vessels. The black square indicates magnified area. The black arrow indicates new blood vessels. The blue arrow indicates cartilage structure. S indicates scaffold. Scale bar = 200 μm. (B) Numbers of neovascularization in each group. (C) Masson trichrome staining showed the mature and immature bone tissues in the new bone. The black square indicates magnified area. Scale bar = 200 μm. (D) Quantitatively analyzed area of newly formed bone tissue. IMBT refers to immature bone tissue, while MBT refers to mature bone tissue. Data are represented as mean ± SD ($n = 3$; the black * indicates total newly formed bone tissue, and the red * indicates mature bone tissue; *$P < 0.05$, **$P < 0.01$, ***$P < 0.001$, ****$P < 0.0001$). (For interpretation of the references to colour in this figure legend, the reader is referred to the Web version of this article.)

and elicit vascular endothelial dysfunction, leading to a severe impact on blood vessel regeneration [24,25]. Therefore, we observe that angiogenesis is essential for osteonecrosis therapy, and there exists a close relationship between VEGF and angiogenesis. Platelet endothelial cell adhesion molecule-1 (CD31) is usually found in vascular endothelial cells and can be used to evaluate angiogenesis [26,27]. We chose VEGF and CD31 as the marker proteins to analyze angiogenesis. There were very few VEGF- and CD31-positively-stained capillaries in the control group during new bone formation (Fig. 5). However, the PLGA/nHA_{10} and PLGA/nHA_{30} groups showed more positive veins with luminal appearance. The PLGA/nHA_{30}^{VEGF} group showed the most and strongest positively-stained capillaries during new bone formation, and these were densely distributed. Relative quantitative analysis of the VEGF- and CD31-positively-stained capillaries in the new bone tissue showed that the expression of the two proteins in the PLGA/nHA_{30}^{VEGF} group was highest in the four groups, reaching more than two times the value of the undecorated composite scaffold groups ($P < 0.01$), and eleven times (VEGF, $P < 0.001$) and six times (CD31, $P < 0.01$) the values of the control group. VEGF is recognized as a critical regulator of physiological angiogenesis in the process of bone regeneration. Therefore, the synergistic treatment using VEGF and the composite scaffold is an excellent method to counter the revascularization challenges in osteonecrosis.

The superior outcomes obtained using PLGA/nHA_{30}^{VEGF} in bone regeneration after core decompression in the osteonecrosis model were further confirmed by the immunohistochemical results that measured OCN, Runx2, OPN, and Col I. OCN and OPN are important late-stage osteogenic markers. OCN interferes with bone metabolism, affects lipid metabolism, and reduces fat deposition [28], while OPN is involved in bone formation and reconstruction. Runx2 is a specific transcription factor for osteogenic differentiation, which regulates the transcription of many genes and promotes the differentiation of BM-MSCs into osteoblasts. Col I is the main component of organic matrices in bone tissue, and it is closely related to bone remodeling. The expression of these four proteins was significantly higher in the groups of scaffolds, especially PLGA/nHA_{30}^{VEGF}, compared with those of the control (Figs. 6 and 7). After the composite scaffold was functionalized with VEGF, it showed

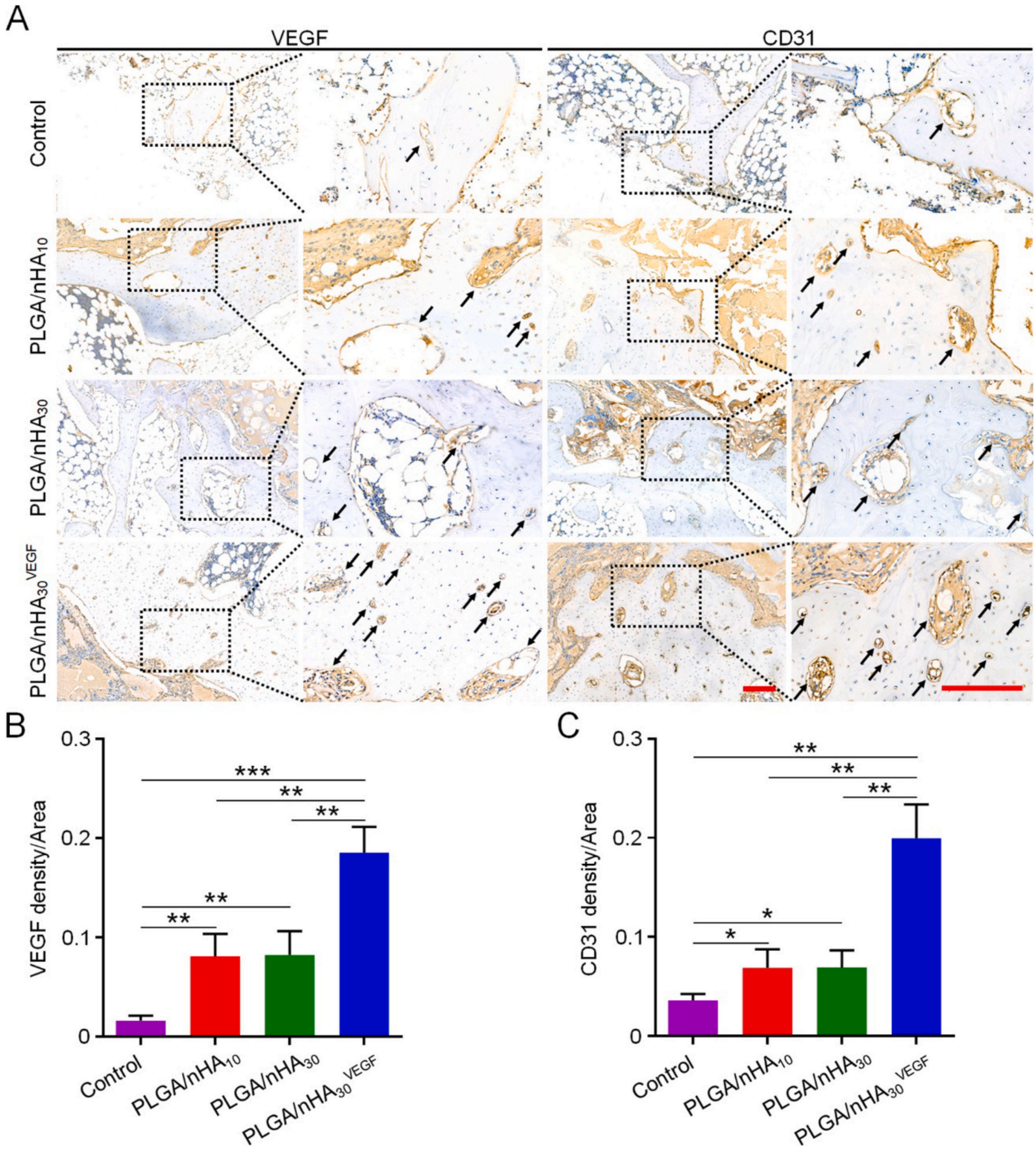

Fig. 5. Immunohistochemical analysis of related protein expression. (A) VEGF and CD31 expression in each group. The black square indicates magnified area. The black arrow indicates positive staining blood vessels. Scale bar = 200 μm. Relative quantification for (B) expression of VEGF and (C) CD31. Data are represented as mean ± SD ($n = 3$; $^{*}P < 0.05$, $^{**}P < 0.01$, $^{***}P < 0.001$, $^{****}P < 0.0001$).

more intense staining than previous results, and the positive staining area was also more extensive. Quantitatively, the value of OCN expression for the PLGA/nHA$_{30}$^{VEGF} group was 0.34, which was higher than those for the other three groups. The values for the PLGA/nHA$_{10}$ and PLGA/nHA$_{30}$ groups were 0.25 and 0.22, and the value for the control group was the lowest, only 0.13. The Runx2 and Col I expression for the PLGA/nHA$_{10}$ and PLGA/nHA$_{30}$ groups were more than double compared with those of the control group ($P < 0.01$), while the value for the PLGA/nHA$_{30}$^{VEGF} group was four times as much as that for the control group ($P < 0.01$ in Col I, and $P < 0.001$ in Runx2). Similarly, the expression of OPN in the PLGA/nHA$_{30}$^{VEGF} group was about three times higher than that in the undecorated composite scaffold groups ($P < 0.01$) and seven times higher than that in the control group ($P < 0.001$).

OCN, Runx2, OPN, and Col I are essential markers of osteogenesis, which all show increased expression levels in bone repair, especially in the late stage (12 weeks) [29–32]. Considering the role and influence of these four proteins in bone tissue regeneration and reconstruction, we believe that the biofunctionalized composite scaffold has excellent osteogenic ability. This was mainly attributed to the addition of synthetic nHA and VEGF. Synthetic nHA has excellent osteoconductivity and osteoinductivity, induces osteogenic differentiation of BM-MSCs, and promotes new bone formation [9,10]. VEGF affects angiogenesis, thereby accelerating bone reconstruction.

In summary, PLGA/nHA$_{30}$^{VEGF} had the best repair effect, and this should be attributed to the increase of nHA content and VEGF biofunctionalization.

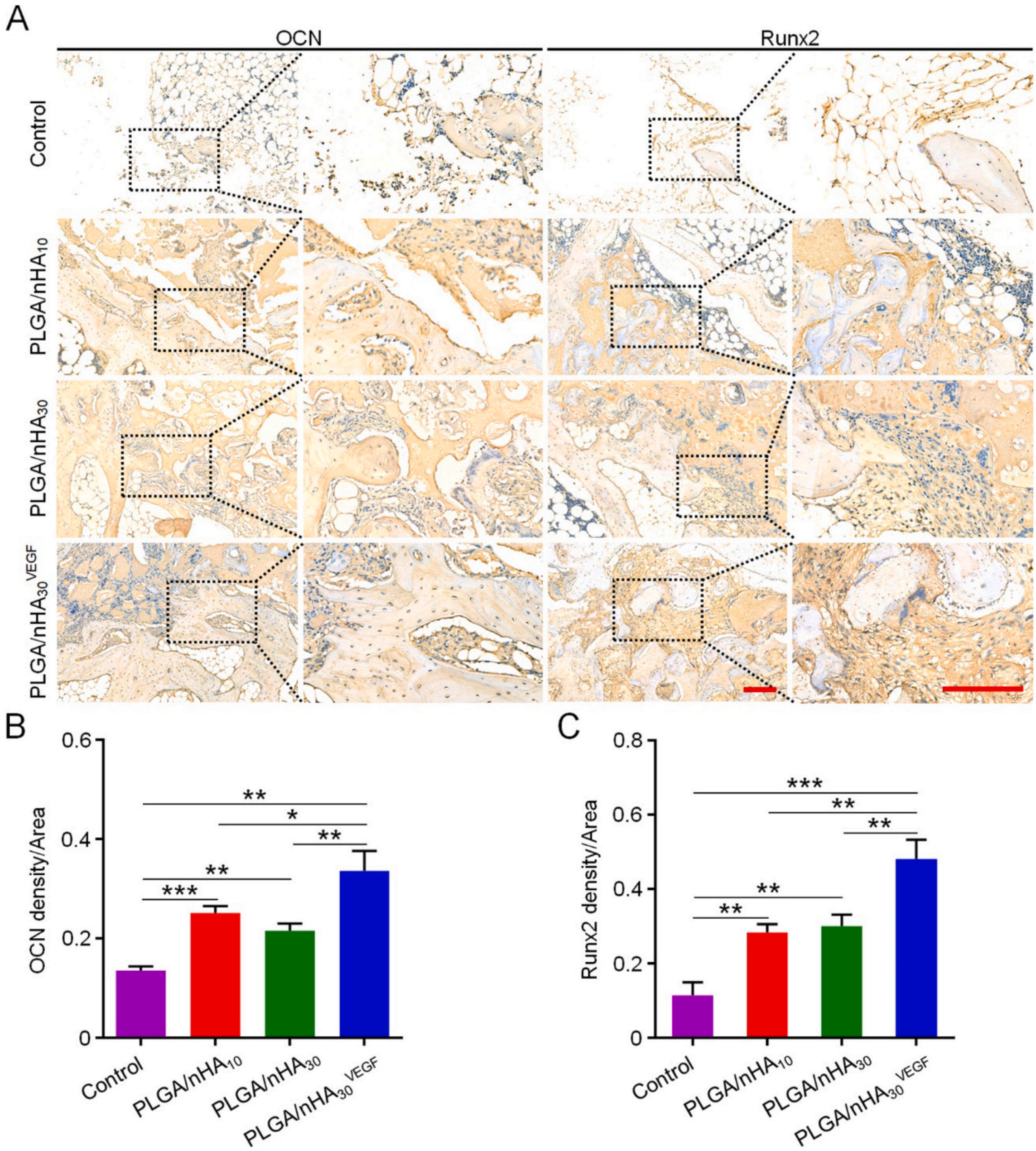

Fig. 6. Immunohistochemical analysis of related protein expression. (A) OCN and Runx2 expression in each group. The black square indicates magnified area. Scale bar = 200 μm. Relative quantification for (B) expression of OCN and (C) Runx2. Data are represented as mean ± SD ($n = 3$; $^{*}P < 0.05$, $^{**}P < 0.01$, $^{***}P < 0.001$).

3.3. Biofunctionalized scaffold corrected metabolic microenvironments of bone tissue

The ideal biomaterial is considered a dynamic control system that can rectify the unfavorable factors in the microenvironments, thereby accurately coordinating various events in the bone regeneration process [33]. In this study, we used a combination of the UPLC-MS/MS detection platform, a self-built database, and multivariate statistical analysis to study the metabolomic and lipidomic differences between groups. The total ion chromatography of the mass spectrometry detection and orthogonal partial least squares-discriminant analysis demonstrated the stability and repeatability of our results. The differential metabolites were screened based on the preset fold change, VIP value, and *P*-value, and then the next step of the analysis was performed (Fig. S6–S9, Supplementary data).

3.3.1. Screening of potential metabolites and metabolism pathway

We analyzed trends in the relative content changes of metabolites in different groups, standardized and centralized the relative contents of differential metabolites, and then performed K-means clustering analysis to visually observe the changing trends of differential metabolites in the three groups (Fig. 8A). From the results, we observed that the expression levels of many metabolites tended to normalize after treatment with the biofunctionalized composite scaffold, which means that PLGA/nHA_{30}^{VEGF} restored abnormal metabolite levels, caused by osteonecrosis, back to normal. Based on the above results, we screened out the differential metabolites related to osteonecrosis. To observe the changes in metabolite levels, we normalized these metabolites and generated a cluster heat map (Fig. 8B).

The levels of three metabolites derived from hippuric acid, caffeic acid, and shikimic acid were significantly downregulated in the model group and recovered after treatment. Hippuric acid inhibits the

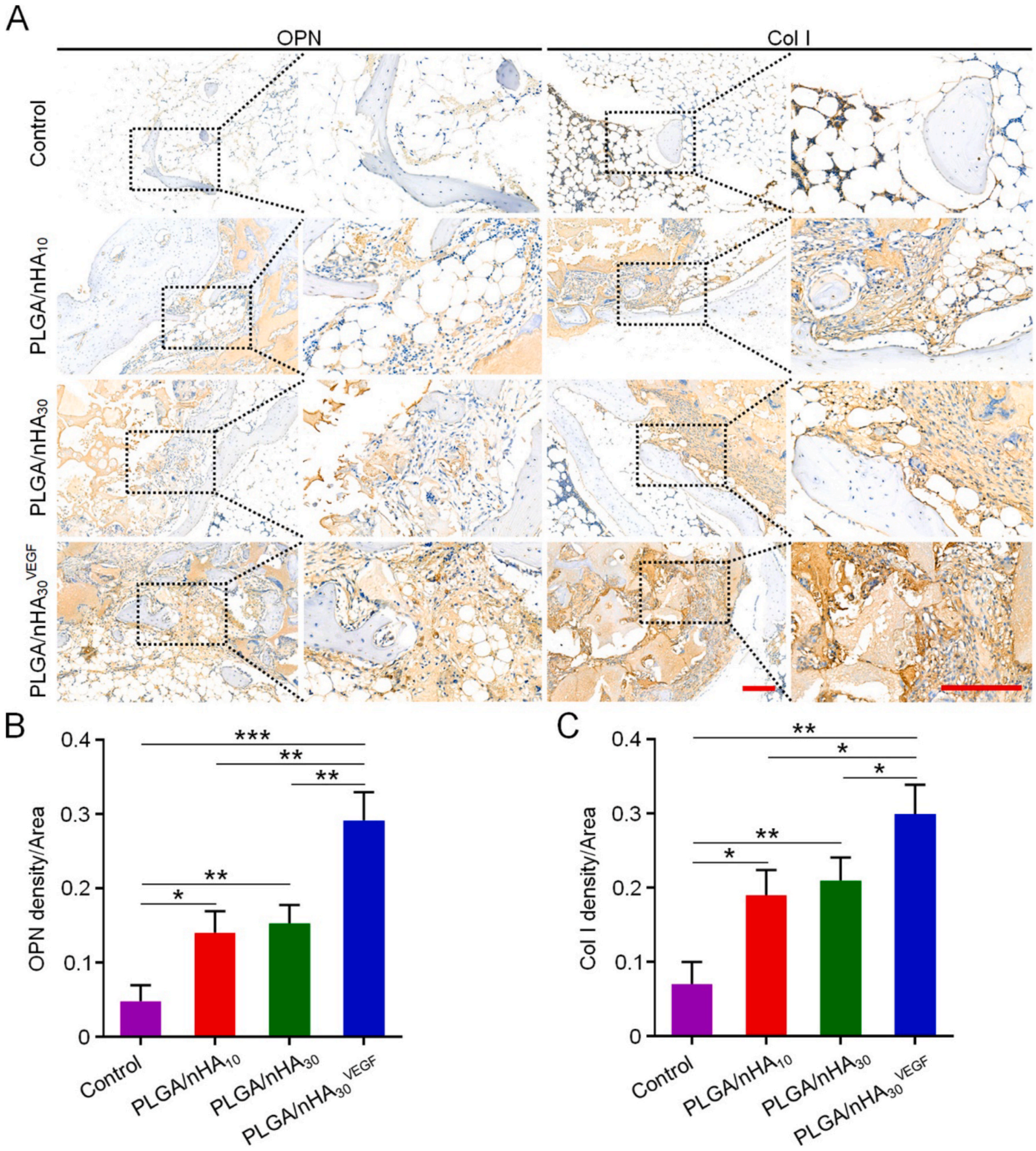

Fig. 7. Immunohistochemical analysis of related protein expression. (A) OPN and Col I expression in each group. The black square indicates magnified area. Scale bar = 200 μm. Relative quantification for (B) expression of OPN and (C) Col I. Data are represented as mean ± SD ($n = 3$; *$P < 0.05$, **$P < 0.01$, ***$P < 0.001$).

formation and activity of osteoclasts through the RANKL/RANK pathway while promoting osteoblast differentiation and bone deposition [34]. Caffeic acid and shikimic acid interfered with osteoclast activity in a similar manner [35,36]. Furthermore, L-serine and cystine levels significantly increased in the model group and slightly decreased in the treatment group. Gang *et al.* showed that L-serine increased in osteonecrosis, and L-serine promoted the formation of osteoclasts, thereby inducing bone resorption, which might be related to the effect of L-serine on RANKL signal transduction [37]. Cystine has the effect of negatively regulating Runx2, thereby affecting bone regeneration, a finding which is supported by our immunohistochemistry results [38].

Trigonelline showed decreased expression in knee osteoarthritis, which was one of the secondary lesions of osteonecrosis [39]. In our study, trigonelline was significantly downregulated in the model group and partially recovered after treatment. Similar expression trends were observed using sepiapterin, the precursor of NO synthase cofactor BH4, promoting NO synthesis and angiogenesis [40]. Oxidative stress and vascular damage caused by NO decline are one of the pathological mechanisms of osteonecrosis. These changes seemed to be related to the abnormal levels of these metabolites in the model group. Therefore, we inferred that local treatment with biofunctionalized composite scaffolds improved the poor pathological microenvironments caused by osteonecrosis.

Differential metabolism interacts in the organism to form different pathways. We made a signal network diagram to study the relationship between differential metabolites (Fig. S10, Supplementary data). The networks were linked with differentially expressed metabolites. Then, we used the KEGG pathway database (http://www.kegg.jp/kegg/pathway.html) to classify the affected related metabolic pathways (Fig. 8C). When we compared the normal and model groups, some metabolic pathways, such as riboflavin metabolism, pyrimidine metabolism, folate metabolism, ABC transporter, ferroptosis, galactose

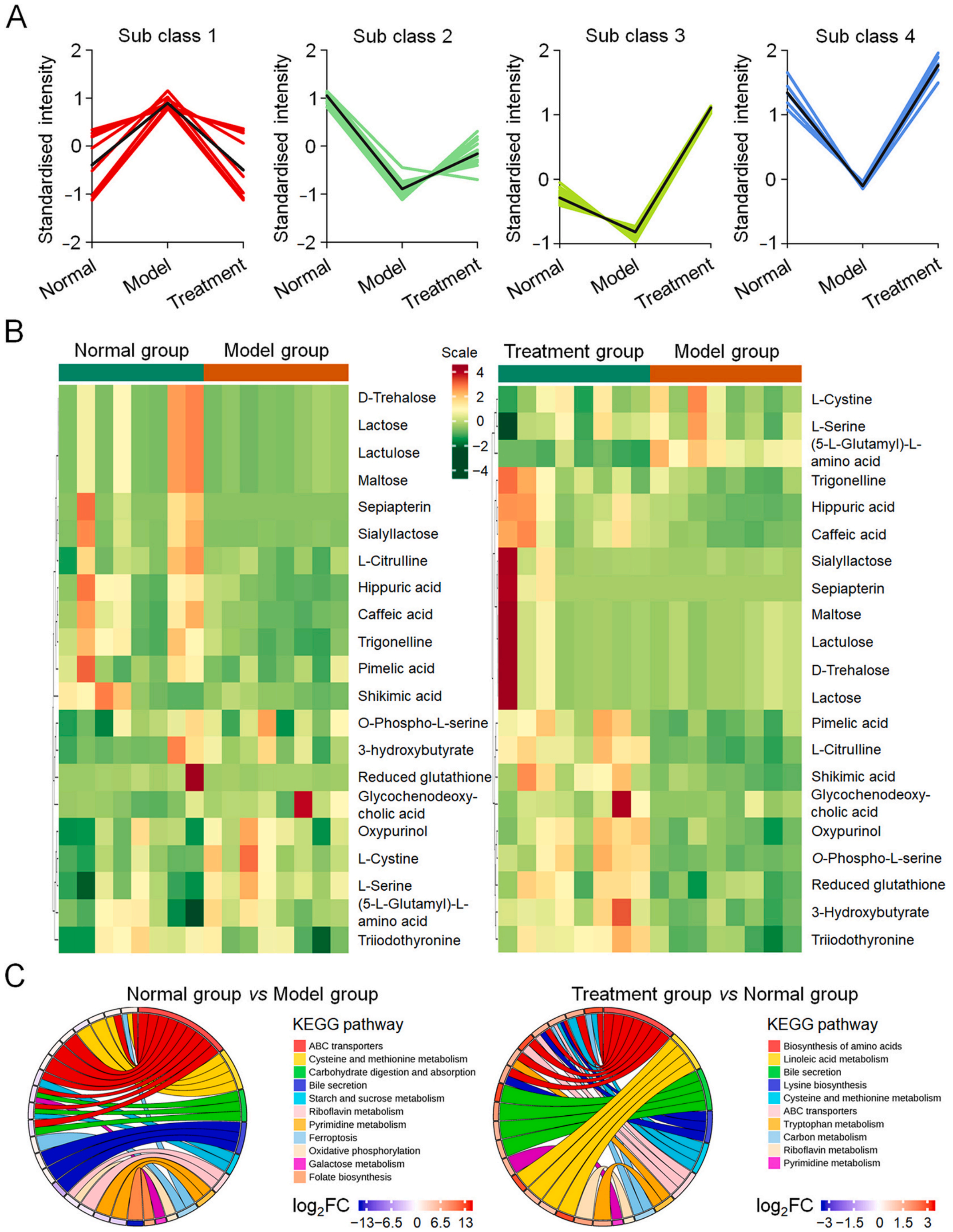

Fig. 8. Screening of potential metabolites and metabolism pathway analysis. (A) K-means analysis reflected the change trends of the relative contents of metabolites in the normal, model, and treatment groups. (B) Cluster heat maps of osteonecrosis-related metabolites with significant differences. (C) Circos plots depicted partially related classification of affected metabolic pathways.

metabolism, carbohydrate digestion and absorption metabolism, oxidative phosphorylation, and cysteine and methionine metabolism, were disordered. The degree of influence of these metabolic pathways decreased or even disappeared when comparing the normal and treatment groups.

Many reports have confirmed that metabolic pathway disorders associated with pyrimidine metabolism, cysteine and methionine metabolism, and galactose metabolism are related to steroid therapy and osteonecrosis [37,41]. Additionally, members of the ABC transporter family are involved in various cell regulation processes, such as lipid transport and iron metabolism. Additionally, ABC transporter disorders have appeared in the rat osteoporosis model [42]. This evidence demonstrated that the ABC transporter was closely related to bone metabolism. Ferroptosis is one of the main mechanisms of cell death associated with ischemic organ damage. It promotes the accumulation of deadly reactive oxygen species produced by lipid peroxidation products and iron metabolism. This action may disrupt lipid metabolism and promote oxidative stress, resulting in osteonecrosis [41,43].

3.3.2. *Screening of potential lipid metabolites and metabolic pathways*

Impaired fat metabolism is one of the leading causes of osteonecrosis. Osteonecrosis induces hypertrophy and hyperplasia of fat cells and generates fat embolism, which further causes increased intraosseous pressure and ischemia to form a vicious circle. VEGF has the effect of rectifying abnormal lipogenesis. Therefore, we used lipidomic profiling to explore the regulation of biofunctionalized composite scaffolds on fat metabolism disorders in osteonecrosis.

After screening lipid metabolites and performing K-means clustering analysis (Fig. 9A), we once again found that many lipid metabolites were abnormal in the model group compared with the normal group, and these abnormalities were corrected after treatment with PLGA/nHA$_{30}$-^{VEGF}. When the normal and model group were compared, 11 glycerophospholipid metabolites in the model group were downregulated, while other glycerolipids and fatty acyl metabolites were upregulated (Fig. 9B). In contrast, 160 glycerophospholipids and sphingomyelin metabolites in the treatment group were upregulated compared with these of the model and treatment groups. The metabolites of glycerophospholipids and glyceride accounted for 42.3% and 50.0% of the total metabolites in osteonecrosis, respectively. In contrast, glycerophospholipids accounted for 62.8% and glyceride for 16.5% under the management of PLGA/nHA$_{30}$^{VEGF}. Glycerophospholipids are the main components of cell membranes, which regulate the transport process, protein function, signal transduction, affect the function and metabolism of lipoproteins, promote fat metabolism, and improve blood circulation. Ren *et al.* observed decreased glycerophospholipids in osteonecrosis and believed this was related to cell apoptosis [44]. Moreover, compared with the model group, the treatment group had nine oxidized lipid metabolites that were significantly upregulated. Oxidized lipids are oxidative metabolites produced by unsaturated fatty acids under the action of specific enzymes, which promote tissue repair and cell proliferation, improving vascular permeability and anti-oxidative stress.

Once again, we used the KEGG pathway database to analyze the metabolic pathways related to osteonecrosis (Fig. 9C). These metabolic pathways included glycerophospholipid metabolism, arachidonic acid metabolism, linolenic acid metabolism, α-linolenic metabolism, and phosphatidylinositol signaling metabolism, which were disordered in the model group. After scaffold implantation, the influence of osteonecrosis on some of these pathways was reduced.

Arachidonic acid, linolenic acid, and α-linolenic acid are unsaturated fatty acids, reducing blood viscosity, improving blood microcirculation, esterifying cholesterol, and lowering blood cholesterol triglycerides. The latest research showed that unsaturated fatty acids were positively correlated with bone density [45]. Xia *et al.* suggested that arachidonic

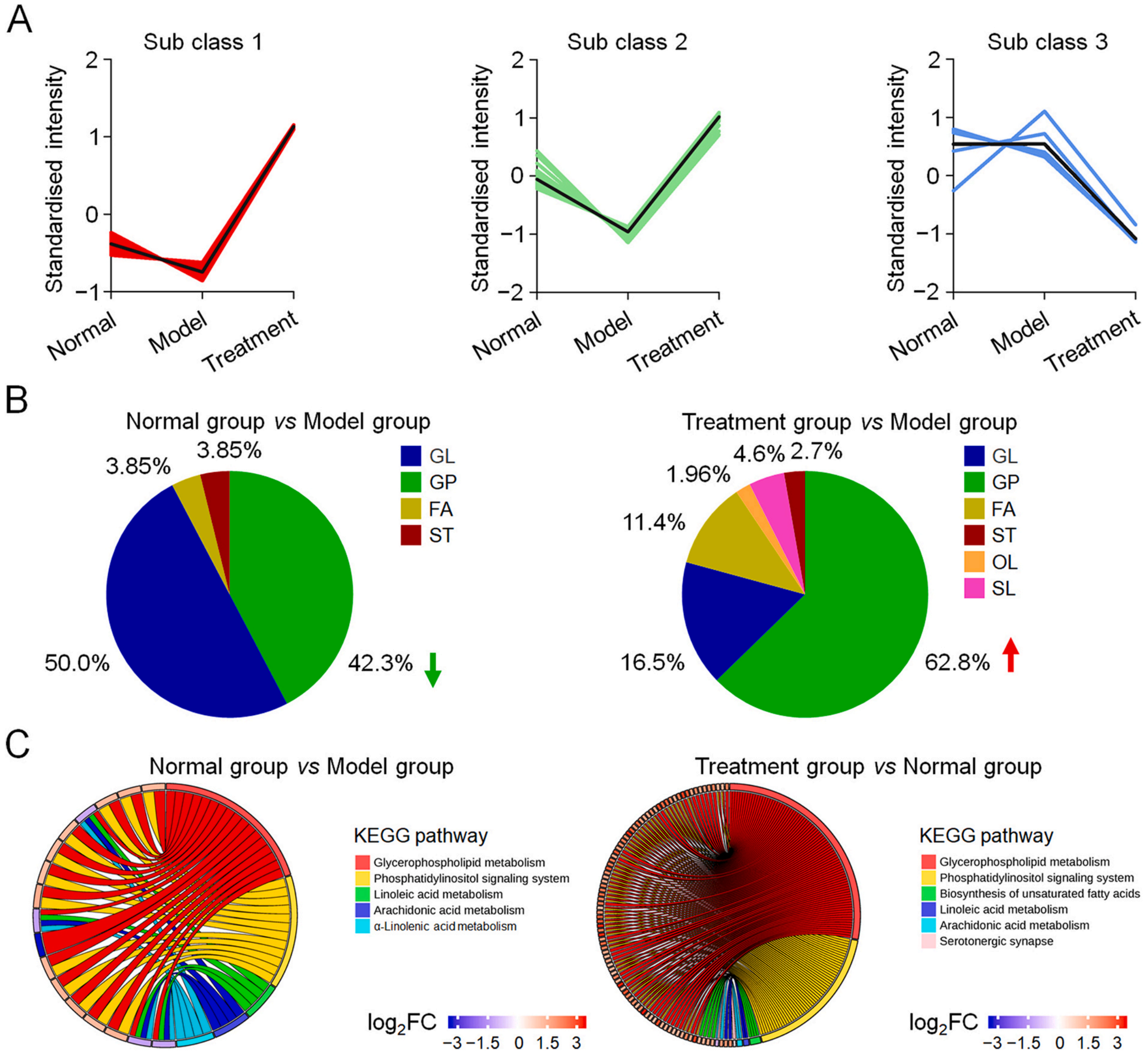

Fig. 9. Screening of potential lipid metabolites and metabolism pathway analysis. (A) K-means analysis reflected the change trends of the relative contents of lipid metabolites in different groups. (B) Proportions of various differential lipid metabolites. Abbreviation directory: FA, fatty acyl; GL, glyceride; GP, glycerophospholipids, OL, oxidized lipids; SL, sphingolipid; ST, sterols. (C) Circos plots depict, partially related classification of affected metabolic pathways.

acid metabolism was disordered after the rats were given steroid therapy [46]. Epoxyeicosatrienoic acid, a metabolite of arachidonic acid, promotes the migration of vascular endothelial cells, aids in the formation of stromal blood vessels, and promotes angiogenesis, and all these factors may be related to VEGF expression [47]. Simultaneously, arachidonic acid is one of the main substances producing prostaglandins, and the latter has the effect of controlling bone homeostasis and promoting bone formation [48]. Linoleic acid is a required substance for cholesterol metabolism. α-Linolenic acid is the primary component of cell membranes and biological enzymes, which regulate blood lipids, inhibit cholesterol synthesis, and are resistant to hypoxic microenvironments. The changes in lipid metabolites and metabolic pathways mean that the biofunctionalized composite scaffold has a significant regulatory effect on abnormal lipid metabolism in osteonecrosis.

We inferred that our osteonecrosis model was successfully established on a metabolic level by integrating the metabolomic and lipidomic profiling results. The application of a biofunctionalized composite scaffold may effectively resist a variety of adverse microenvironments in osteonecrosis.

4. Conclusion

The biofunctionalized composite scaffold PLGA/nHA$_{30}$$^{\mathrm{VEGF}}$ with appropriate physicochemical properties was prepared by coating the porous PLGA/nHA$_{30}$ with VEGF. Compared with the undecorated scaffolds, PLGA/nHA$_{30}$$^{\mathrm{VEGF}}$ had a similar pore size and porosity, but better hydrophilicity and degradability. With the sustained release of VEGF, PLGA/nHA$_{30}$$^{\mathrm{VEGF}}$ significantly promoted the new bone formation and neo-angiogenesis in the rabbit osteonecrosis model. Furthermore, metabolomic and lipidomic provided valuable insights into the microenvironmental disorders of osteonecrosis, which suggested that PLGA/nHA$_{30}$$^{\mathrm{VEGF}}$ may reverse the adverse microenvironments of osteonecrosis by metabolism regulation, overcome bone regeneration obstacles, and play a role in osteonecrosis therapy. Moreover, the metabolomic and lipidomic studies discover the specific biomarkers of osteonecrosis and guide osteonecrosis therapy, and it is a promising method for evaluating the effectiveness of diagnosis and treatment. In summary, using its function of promoting osteoconduction, potentiating angiogenesis, and regulating the metabolic microenvironments, the biofunctionalized composite scaffold effectively potentiated the therapy efficacy of early osteonecrosis.

Declaration of competing interest

The authors declare that they have no known competing financial interests or personal relationships that could have appeared to influence the work reported in this paper.

CRediT authorship contribution statement

Tongtong Zhu: Conceptualization, Methodology, Formal analysis, Investigation, Writing – original draft, Writing – review & editing. **Mengyang Jiang:** Writing – review & editing. **Mingran Zhang:** Writing – review & editing. **Liguo Cui:** Resources. **Xiaoyu Yang:** Writing – review & editing. **Xukai Wang:** Writing – review & editing. **Guangyao Liu:** Conceptualization, Writing – review & editing, Supervision, Project administration, Funding acquisition. **Jianxun Ding:** Conceptualization, Writing – review & editing, Supervision, Project administration, Funding acquisition. **Xuesi Chen:** Writing – review & editing.

Acknowledgments

This study was financially supported by the National Natural Science Foundation of China (Grant Nos. 52022095, 51973216, 51873207, 51803006, and 51833010), the Provincial Health Specific Project of Jilin Province (Grant Nos. JLSWSRCZX2020-0021, 2018SCZ018, and SCZSY201710), the Specific Project for Health Research Talents of Jilin Province (Grant No. 2019SCZ025), the Science and Technology Development Program of Jilin Province (Grant Nos. 20200404182YY, 20200201478JC, and 20190303154SF), the Youth Innovation Promotion Association of Chinese Academy of Sciences (Grant No. 2019230), and the State Key Laboratory of Advanced Technology for Materials Synthesis and Processing (Wuhan University of Technology) (Grant No. 2020-KF-5). In addition, the authors are grateful to Wuhan Metware Biotechnology Co., Ltd, Wuhan, P. R. China, for the assistance in metabolomic analysis and Dr. Di Li from the First Hospital of Jilin University, P. R. China, for the valuable discussion.

Appendix A. Supplementary data

Supplementary data to this article can be found online at https://doi.org/10.1016/j.bioactmat.2021.08.005.

Data availability

All relevant data supporting the findings of this study are either included within the article and its Supplementary Information files or available upon request from the corresponding author.

References

[1] J. Li, Z. Ge, W. Ji, N. Yuan, K. Wang, The proosteogenic and proangiogenic effects of small extracellular vesicles derived from bone marrow mesenchymal stem cells are attenuated in steroid-induced osteonecrosis of the femoral head, BioMed Res. Int. 2020 (2020) 4176926.

[2] T.T. Zhu, Y.T. Cui, M.R. Zhang, D.Y. Zhao, G.Y. Liu, J.X. Ding, Engineered three-dimensional scaffolds for enhanced bone regeneration in osteonecrosis, Bioact. Mater. 5 (3) (2020) 584–601.

[3] G. Chen, Q. Wang, Z. Li, Q. Yang, Y. Liu, Z. Du, G. Zhang, Y. Song, Circular RNA CDR1 as promotes adipogenic and suppresses osteogenic differentiation of BMSCs in steroid-induced osteonecrosis of the femoral head, Bone 133 (2020) 115258.

[4] G.Y. Chen, L. Zhong, Q.Y. Wang, Z.Y. Li, J. Shang, Q.W. Yang, Z.W. Du, J.C. Wang, Y. Song, G.Z. Zhang, The expression of chondrogenesis-related and arthritis-related genes in human ONFH cartilage with different Ficat stages, PeerJ 7 (2019), e6306.

[5] K.H. Koo, R. Kim, Y.S. Kim, I.O. Ahn, S.H. Cho, H.R. Song, Y.S. Park, H. Kim, G. J. Wang, Risk period for developing osteonecrosis of the femoral head in patients on steroid treatment, Clin. Rheumatol. 21 (4) (2002) 299–303.

[6] K. Ikeuchi, Y. Hasegawa, T. Seki, Y. Takegami, T. Amano, N. Ishiguro, Epidemiology of nontraumatic osteonecrosis of the femoral head in Japan, Mod. Rheumatol. 25 (2) (2015) 278–281.

[7] Y. Lai, Y. Li, H. Cao, J. Long, X. Wang, L. Li, C. Li, Q. Jia, B. Teng, T. Tang, J. Peng, D. Eglin, M. Alini, D.W. Grijpma, G. Richards, L. Qin, Osteogenic magnesium incorporated into PLGA/TCP porous scaffold by 3D printing for repairing challenging bone defect, Biomaterials 197 (2019) 207–219.

[8] L.Z. Zheng, H.J. Cao, S.H. Chen, T. Tang, W.M. Fu, L. Huang, D.H.K. Chow, Y. X. Wang, J.F. Griffith, W. He, H. Zhou, D.W. Zhao, G. Zhang, X.L. Wang, L. Qin, Blockage of Src by specific siRNA as a novel therapeutic strategy to prevent destructive repair in steroid-associated osteonecrosis in rabbits, J. Bone Miner. Res. 30 (11) (2015) 2044–2057.

[9] L. Benedini, J. Laiuppa, G. Santillán, M. Baldini, P. Messina, Antibacterial alginate/nano-hydroxyapatite composites for bone tissue engineering: Assessment of their bioactivity, biocompatibility, and antibacterial activity, Mater. Sci. Eng. C Mater. Biol. Appl. 115 (2020) 111101.

[10] H. Zhou, A.J. Boys, J.B. Harrod, L.J. Bonassar, L.A. Estroff, Mineral distribution spatially patterns bone marrow stromal cell behavior on monolithic bone scaffolds, Acta Biomater. 112 (2020) 274–285.

[11] D.Y. Zhao, T.T. Zhu, J. Li, L.G. Cui, Z. Zhang, X.L. Zhuang, J.X. Ding, Poly(lactic-*co*-glycolic acid)-based composite bone-substitute materials, Bioact. Mater. 6 (2) (2021) 346–360.

[12] L. Cui, J. Zhang, J. Zou, X. Yang, H. Guo, H. Tian, P. Zhang, Y. Wang, N. Zhang, X. Zhuang, Z. Li, J. Ding, X. Chen, Electroactive composite scaffold with locally expressed osteoinductive factor for synergistic bone repair upon electrical stimulation, Biomaterials 230 (2020) 119617.

[13] Y. Zha, T. Lin, Y. Li, X. Zhang, Z. Wang, Z. Li, Y. Ye, B. Wang, S. Zhang, J. Wang, Exosome-mimetics as an engineered gene-activated matrix induces *in-situ* vascularized osteogenesis, Biomaterials 247 (2020) 119985.

[14] M.O. Wang, C.E. Vorwald, M.L. Dreher, E.J. Mott, M.H. Cheng, A. Cinar, H. Mehdizadeh, S. Somo, D. Dean, E.M. Brey, J.P. Fisher, Evaluating 3D-printed biomaterials as scaffolds for vascularized bone tissue engineering, Adv. Mater. 27 (1) (2015) 138–144.

[15] F.P. Cantatore, E. Crivellato, B. Nico, D. Ribatti, Osteocalcin is angiogenic *in vivo*, Cell Biol. Int. 29 (7) (2005) 583–585.

[16] X.H. Xie, X.L. Wang, H.L. Yang, D.W. Zhao, L. Qin, Steroid-associated osteonecrosis: Epidemiology, pathophysiology, animal model, prevention, and potential treatments (an overview), J. Orthop. Transl. 3 (2) (2015) 58–70.
[17] M. Maruyama, A. Nabeshima, C.C. Pan, A.W. Behn, T. Thio, T. Lin, J. Pajarinen, T. Kawai, M. Takagi, S.B. Goodman, Y.P. Yang, The effects of a functionally-graded scaffold and bone marrow-derived mononuclear cells on steroid-induced femoral head osteonecrosis, Biomaterials 187 (2018) 39–46.
[18] Y.X. Lai, H.J. Cao, X.L. Wang, S.K. Chen, M. Zhang, N. Wang, Z.H. Yao, Y. Dai, X. H. Xie, P. Zhang, X.S. Yao, L. Qin, Porous composite scaffold incorporating osteogenic phytomolecule icariin for promoting skeletal regeneration in challenging osteonecrotic bone in rabbits, Biomaterials 153 (2018) 1–13.
[19] J. Ding, J. Zhang, J. Li, D. Li, C. Xiao, H. Xiao, H. Yang, X. Zhuang, X. Chen, Electrospun polymer biomaterials, Prog. Polym. Sci. 90 (2019) 1–34.
[20] L. Zhang, G.J. Yang, B.N. Johnson, X.F. Jia, Three-dimensional (3D) printed scaffold and material selection for bone repair, Acta Biomater. 84 (2019) 16–33.
[21] Y.X. Huang, J. Ren, C. Chen, T.B. Ren, X.Y. Zhou, Preparation and properties of poly(lactide-*co*-glycolide) (PLGA)/nano-hydroxyapatite (nHA) scaffolds by thermally induced phase separation and rabbit MSCs culture on scaffolds, J. Biomater. Appl. 22 (5) (2008) 409–432.
[22] H. Rezaei, M. Shahrezaee, M. Jalali Monfared, F. Ghorbani, A. Zamanian, M. Sahebalzamani, Mussel-inspired polydopamine induced the osteoinductivity to ice-templating PLGA–gelatin matrix for bone tissue engineering application, Biotechnol. Appl. Biochem. 3 (2020) 185–196.
[23] W.G. Bian, D.C. Li, Q. Lian, W.J. Zhang, L.Z. Zhu, X. Li, Z.M. Jin, Design and fabrication of a novel porous implant with preset channels based on ceramic stereolithography for vascular implantation, Biofabrication 3 (3) (2011), 034103.
[24] T. Iuchi, M. Akaike, T. Mitsui, Y. Ohshima, Y. Shintani, H. Azuma, T. Matsumoto, Glucocorticoid excess induces superoxide production in vascular endothelial cells and elicits vascular endothelial dysfunction, Circ. Res. 92 (1) (2003) 81–87.
[25] W. Zuo, W.S. Guo, H.C. Yu, P. Liu, Q.D. Zhang, Role of junction-mediating and regulatory protein in the pathogenesis of glucocorticoid-induced endothelial cell lesions, Orthop. Surg. 12 (3) (2020) 964–973.
[26] R. Zhao, S.Y. Chen, W.L. Zhao, L. Yang, B. Yuan, S.I. Voicu, A.V. Iulian, X. Yang, X. D. Zhu, X.D. Zhang, A bioceramic scaffold composed of strontium-doped three-dimensional hydroxyapatite whiskers for enhanced bone regeneration in osteoporotic defects, Theranostics 10 (4) (2020) 1572–1589.
[27] P. Gao, B. Fan, X. Yu, W. Liu, J. Wu, L. Shi, D. Yang, L. Tan, P. Wan, Y. Hao, S. Li, W. Hou, K. Yang, X. Li, Z. Guo, Biofunctional magnesium coated Ti_6Al_4V scaffold enhances osteogenesis and angiogenesis *in vitro* and *in vivo* for orthopedic application, Bioact. Mater. 5 (3) (2020) 680–693.
[28] T. Otani, A. Mizokami, T. Kawakubo-Yasukochi, H. Takeuchi, T. Inai, M. Hirata, The roles of osteocalcin in lipid metabolism in adipose tissue and liver, Adv. Biol. Regul. 78 (2020) 100752.
[29] Y. Niu, L. Wang, N. Yu, P. Xing, Z. Wang, Z. Zhong, Y. Feng, L. Dong, C. Wang, An "all-in-one" scaffold targeting macrophages to direct endogenous bone repair in situ, Acta Biomater. 111 (2020) 153–169.
[30] J. Zhang, H. Liu, J.X. Ding, J. Wu, X.L. Zhuang, X.S. Chen, J.C. Wang, J.B. Yin, Z. M. Li, High-pressure compression-molded porous resorbable polymer/hydroxyapatite composite scaffold for cranial bone regeneration, ACS Biomater. Sci. Eng. 2 (9) (2016) 1471–1482.
[31] X. Liu, M.N. George, S. Park, A.L. Miller Ii, B. Gaihre, L. Li, B.E. Waletzki, A. Terzic, M.J. Yaszemski, L. Lu, 3D-printed scaffolds with carbon nanotubes for bone tissue engineering: Fast and homogeneous one-step functionalization, Acta Biomater. 111 (2020) 129–140.
[32] Y.F. Yan, H. Chen, H.B. Zhang, C.J. Guo, K. Yang, K.Z. Chen, R.Y. Cheng, N. D. Qian, N. Sandler, Y.S. Zhang, H.K. Shen, J. Qi, W.G. Cui, L.F. Deng, Vascularized 3D printed scaffolds for promoting bone regeneration, Biomaterials 190 (2019) 97–110.
[33] P. Qiu, M. Li, K. Chen, B. Fang, P. Chen, Z. Tang, X. Lin, S. Fan, Periosteal matrix-derived hydrogel promotes bone repair through an early immune regulation coupled with enhanced angio- and osteogenesis, Biomaterials 227 (2020) 119552.
[34] H. Zhao, O.P. Lazarenko, J.R. Chen, Hippuric acid and 3-(3-hydroxyphenyl) propionic acid inhibit murine osteoclastogenesis through RANKL-RANK independent pathway, J. Cell. Physiol. 235 (1) (2020) 599–610.
[35] X. Chen, X. Li, X. Zhai, X. Zhi, L. Cao, L. Qin, J. Su, Shikimic acid inhibits osteoclastogenesis *in vivo* and *in vitro* by blocking RANK/TRAF6 association and suppressing NF-κB and MAPK signaling pathways, Cell. Physiol. Biochem. 51 (6) (2018) 2858–2871.
[36] E.S.M. Ang, N.J. Pavlos, L.Y. Chai, M. Qi, T.S. Cheng, J.H. Steer, D.A. Joyce, M. H. Zheng, J. Xu, Caffeic acid phenethyl ester, an active component of honeybee propolis attenuates osteoclastogenesis and bone resorption *via* the suppression of RANKL-induced NF-κB and NFAT activity, J. Cell. Physiol. 221 (3) (2009) 642–649.
[37] G. Yang, G. Zhao, J. Zhang, S. Gao, T. Chen, S. Ding, Y. Zhu, Global urinary metabolic profiling of the osteonecrosis of the femoral head based on UPLC–QTOF/MS, Metabolomics 15 (3) (2019) 26.
[38] K. Uno, T. Takarada, Y. Nakamura, H. Fujita, E. Hinoi, Y. Yoneda, A negative correlation between expression profiles of runt-related transcription factor-2 and cystine/glutamate antiporter xCT subunit in ovariectomized mouse bone, J. Pharmacol. Sci. 115 (3) (2011) 309–319.
[39] K.R. Swank, J.E. Furness, E.A. Baker, C.K. Gehrke, S.P. Biebelhausen, K.C. Baker, Metabolomic profiling in the characterization of degenerative bone and joint diseases, Metabolites 10 (6) (2020) 223.
[40] T. Shimazu, H. Otani, K. Yoshioka, M. Fujita, T. Okazaki, T. Iwasaka, Sepiapterin enhances angiogenesis and functional recovery in mice after myocardial infarction, Am. J. Physiol. Heart Circ. Physiol. 301 (5) (2011) H2061–H2072.
[41] J. Wu, Y. Du, J. Song, X. Dang, K. Wang, Y. Wen, F. Zhang, R. Liu, Genome-wide DNA methylation profiling of hip articular cartilage identifies differentially methylated loci associated with osteonecrosis of the femoral head, Bone 127 (2019) 296–304.
[42] M. Ye, C. Zhang, W. Jia, Q. Shen, X. Qin, H. Zhang, L. Zhu, Metabolomics strategy reveals the osteogenic mechanism of yak (Bos grunniens) bone collagen peptides on ovariectomy-induced osteoporosis in rats, Food Funct 11 (2) (2020) 1498–1512.
[43] Y. Xie, W. Hou, X. Song, Y. Yu, J. Huang, X. Sun, R. Kang, D. Tang, Ferroptosis: Process and function, Cell Death Differ. 23 (3) (2016) 369–379.
[44] X. Ren, W. Fan, Z. Shao, K. Chen, X. Yu, Q. Liang, A metabolomic study on early detection of steroid-induced avascular necrosis of the femoral head, Oncotarget 9 (8) (2018) 7984–7995.
[45] J. Huang, Y.P. Hu, X.F. Tong, L. Zhang, Z.W. Yu, Z.X. Zhou, Untargeted metabolomics revealed therapeutic mechanisms of icariin on low bone mineral density in older caged laying hens, Food Funct 11 (4) (2020) 3201–3212.
[46] T. Xia, X. Dong, L. Lin, Y. Jiang, X. Ma, H. Xin, Q. Zhang, L. Qin, Metabolomics profiling provides valuable insights into the underlying mechanisms of Morinda officinalis on protecting glucocorticoid-induced osteoporosis, J. Pharmaceut. Biomed. Anal. 166 (2019) 336–346.
[47] S.Y. Cheranov, M. Karpurapu, D. Wang, B. Zhang, R.C. Venema, G.N. Rao, An essential role for SRC-activated STAT-3 in 14,15-EET–induced VEGF expression and angiogenesis, Blood 111 (12) (2008) 5581–5591.
[48] H. Chen, B. Hu, X. Lv, S. Zhu, G. Zhen, M. Wan, A. Jain, B. Gao, Y. Chai, M. Yang, X. Wang, R. Deng, L. Wang, Y. Cao, S. Ni, S. Liu, W. Yuan, H. Chen, X. Dong, Y. Guan, H. Yang, X. Cao, Prostaglandin E2 mediates sensory nerve regulation of bone homeostasis, Nat. Commun. 10 (1) (2019) 181.